Layered Control for Multi-Use Battery Storage

Jacco Reuling, Juan Camilo López, Gerwin Hoogsteen, Johann L. Hurink
Faculty of EEMCS, University of Twente, Enschede, The Netherlands
e-mail: j.reuling@utwente.nl; j.c.lopezamezquita@utwente.nl; g.hoogsteen@utwente.nl; j.l.hurink@utwente.nl

Abstract—This work presents a layered control strategy for multi-use battery energy storage systems (BESS) that enables simultaneous market-driven operation and grid-aware constraint enforcement. Building on the free-flexibility concept of Nykamp et al., we construct a time-varying feasible flexibility volume using load forecasts, and integrate it into a rolling-horizon MILP for setpoint adaptation. A complementary real-time constraint (RTC) layer ensures instantaneous grid-limit compliance despite forecast errors. The full control architecture is implemented within a Digital Twin environment and experimentally validated on two grid-connected batteries in a laboratory microgrid. Results across multiple grid-limit scenarios show that (i) forecast-based free-flexibility planning effectively prevents predicted violations, (ii) the RTC layer is essential for mitigating unforeseen load deviations, and (iii) forecast uncertainty can lead to state-of-charge drift unless explicitly addressed. These findings demonstrate the practical viability of real-time multi-objective BESS control and highlight the need for uncertainty-aware planning mechanisms.

Index Terms—Battery energy storage systems, Digital Twin, model predictive control, distribution grid constraints, flexibility services

I. INTRODUCTION

The accelerating integration of distributed energy resources (DERs) is imposing unprecedented strains on distribution grids. For example, in the Netherlands, recent analysis estimates that grid investment requirements could rise to 195 billion in 2040 due to electrification and renewable integration. [1]. While energy storage systems, particularly battery energy storage systems (BESS), are widely recognized as a promising solution to defer such costly upgrades and manage local volatility, their effectiveness depends on how they are controlled. Simply operating batteries for market profit without regard for local network limits can exacerbate grid stress. Studies show that uncoordinated market-only battery dispatch (driven by wholesale price signals) can actually increase peak loads and reinforcement needs due to the poor alignment of market signals with local grid conditions [2], [3]. This challenge calls for control strategies that intelligently balance multiple objectives (economic and technical) for battery operation while respecting distribution constraints.

One promising direction is the "multi-use" of batteries, where a single BESS provides services to more than one stakeholder or purpose (e.g. simultaneously pursuing energy arbitrage and distribution peak shaving). A multi-use approach seeks to combine applications for enhanced overall value. Prior work has demonstrated the potential of multi-use BESS operation provided that grid constraints are proactively accounted for. Nykamp et al. introduced a method to forecast day-ahead distribution loading and delineate the battery's "free flexibility" [4]. The set of charging/discharging trajectories that remain feasible after reserving capacity for local peak-shaving. This yields a time-varying 3D flexibility envelope (power vs. energy vs. time) within which a third-party operator (e.g. an aggregator) can dispatch the battery for market purposes without violating the transformer limits. Such studies prove that coordinated multi-objective control can unlock significant value from storage safely. However, most implementations so far rely on off-line scheduling (e.g. day-ahead planning with fixed reserve margins) and do not demonstrate a real-time closed-loop control that continuously adapts to forecast errors and unexpected events.

Implementing a truly dynamic battery energy management system (EMS) for multi-objective operation requires advanced methods that merge forecasting, optimization, and feedback control. Digital twin (DT) technology offers a path to such operation. A DT is a live, virtual replica of the physical system that continuously synchronizes with real-world data and simulations, enabling proactive monitoring, predictive analytics, and control evaluation. Recent frameworks formalize DTs for cyber-physical energy systems by integrating state estimation, load/RES forecasting, and optimization [5], [6]. In the context of multi-use BESS control, a DT can operationalize the free-flexibility concept in a rolling horizon: it forecasts grid conditions, constructs a feasible flexibility envelope, and supervises dispatch while aligning the virtual model with the actual system state. Despite this promise, the literature still lacks practical demonstrations of DT-enabled control that performs continuous multi-objective optimization with real-time constraint enforcement in operating microgrids [6].

This work specifically operationalizes and experimentally validates the free-flexibility concept introduced by Nykamp et al. [4] by integrating it into a rolling-horizon MILP framework and deploying it in real-time on physical hardware. We further demonstrate that forecast-based planning alone is insufficient in practice due to persistent forecast uncertainty. This necessitates a complementary real-time constraint layer.

- Practical validation of free flexibility. We operationalize Nykamp's free-flexibility concept by constructing a forecast-based, time-varying flexibility volume and validating it in closed loop within a Digital Twin (DT).
- Layered constraint-aware control architecture within a Digital Twin. We design a hierarchical control scheme combining a Forecast-Based Constraint (FBC) planning layer with a Real-Time Constraint (RTC) safety layer, coordinated through a Digital Twin that synchronizes forecasts, measurements, and state updates.

- Experimental validation on physical battery systems. The proposed control method is implemented and evaluated on two grid-connected battery systems in a laboratory microgrid environment, under multiple grid capacity scenarios, demonstrating closed-loop feasibility of combining market-driven dispatch and grid-aware constraint handling.

This work is relevant for microgrid operators and aggregators aiming to maximize revenue from BESS without jeopardizing local grid reliability, and for distribution network operators (DSOs) and transmission system operators (TSOs) interested in leveraging customer-owned storage for grid support.

II. METHODOLOGY

The proposed control system is implemented within a Digital Twin (DT) environment, consistent with the modular and synchronized DT architectures described in [6] and the CPES mathematical framework in [5]. The DT maintains a dynamic state representation of the battery (state-of-charge), integrates forecasting models for exogenous variables, constructs the feasible flexibility volume (Section II-A), and solves a rolling-horizon optimization to determine battery setpoints (Section II-B). Real-time measurements synchronize the DT with the physical system, while the RTC layer ensures constraint-safe actuation. Thus, all decision-making and forecasting occur inside the DT.

A. Construction of the Feasible Flexibility Volume

This section describes the construction of the time-varying feasible operating space for the battery energy storage system. The objective is to characterize, at each discrete time step t, the set of feasible battery power p_t and battery energy e_t such that (i) the transformer grid limit is not violated at any time, and (ii) sufficient battery energy capacity is reserved to ensure that future import peaks can be shaved and future export peaks can be absorbed. The union of these feasibility sets across time forms a three-dimensional flexibility volume, following the free-flexibility concept in [4].

1) Notation: Let $t = 0, \ldots, T - 1$ denote discrete time steps of duration Δt (h). The net load forecast at the point of common coupling is denoted l_t (kW), with the convention that positive values indicate net import from the grid and negative values indicate net export. The battery setpoint p_t (kW) is positive when discharging and negative when charging. The battery energy e_t (kWh) is constrained by the nominal capacity $E_{\max}$, and the charge/discharge power is limited by the power rating $P_{\max}$. The distribution transformer grid limit is given by $G > 0$, yielding the constraint

$$|l_t + p_t| \leq G, \qquad \forall t. \tag{1}$$

2) Power Feasibility: Given (1), the instantaneous feasible battery power at each time step is

$$
\begin{aligned}
p_t^{\max} &= \min\{P_{\max}, \ G - l_t\}, \\
p_t^{\min} &= \max\{-P_{\max}, \ -G - l_t\}.
\end{aligned}
\tag{2}
$$

These bounds represent the available "headroom" for discharge ($p_t^{\max}$) and charge ($p_t^{\min}$) without violating the transformer limit.

3) Energy Feasibility via Future Reserve Requirements: To ensure that the battery retains enough stored energy to shave future import peaks, we define a forward-looking reserve:

$$R_t^{\mathrm{imp}} = \sum_{\tau=t}^{\tau_\uparrow(t)} \max(l_\tau - G, 0)\, \Delta t, \tag{3}$$

where $\tau_\uparrow(t)$ is the first future time in which $l_\tau \leq G$. This yields the minimum required battery energy:

$$e_t^{\min} = R_t^{\mathrm{imp}}. \tag{4}$$

Similarly, to preserve enough empty capacity to absorb future export peaks, we define

$$R_t^{\mathrm{exp}} = \sum_{\tau=t}^{\tau_\downarrow(t)} \max(-G - l_\tau, 0)\, \Delta t, \tag{5}$$

where $\tau_\downarrow(t)$ is the first future time in which $l_\tau \geq -G$. This yields the maximum feasible energy:

$$e_t^{\max} = E_{\max} - R_t^{\mathrm{exp}}. \tag{6}$$

4) Time-Indexed Feasible Space and 3D Flexibility Volume: The feasible operating region at each time step is therefore the rectangle

$$\mathcal{F}_t = \left\{ (p_t, e_t) \ : \ p_t^{\min} \leq p_t \leq p_t^{\max}, \ e_t^{\min} \leq e_t \leq e_t^{\max} \right\}, \tag{7}$$

and the overall feasible flexibility volume is the union over the time axis:

$$\mathcal{V} = \bigcup_{t=0}^{T-1} \{t\} \times \mathcal{F}_t. \tag{8}$$

The combined feasible region $\mathcal{V}$ forms a time-indexed flexibility volume from which feasible dispatch trajectories can be selected. This flexibility volume is later used in the rolling-horizon MILP controller (see Figure 1 and Section II-B). Any battery power and energy trajectory that lies entirely within $\mathcal{V}$ is guaranteed to respect both the grid capacity limit and the required future reserve capacity.

Figure 1 illustrates how the feasible flexibility volume is used within the overall control architecture. Business logic or market services define high-level battery steering objectives, expressed as desired real and reactive power setpoints. These setpoints are then passed to a rolling-horizon MILP optimization, which ensures that the selected power trajectory remains within the time-varying feasible flexibility volume derived in Section II-A. The resulting feasible dispatch commands are then applied to the physical battery inverter. In this way, the flexibility volume acts as a constraint layer that ensures grid-compliant operation while still allowing external objectives such as peak shaving, arbitrage, or reactive power support to be pursued.

Intuitively, the flexibility volume defines how much the battery can charge or discharge at each point in time while still preserving the ability to avoid future transformer overloads. Any control strategy that stays inside this volume is guaranteed to remain grid safe.

Algorithm 1: Construction of the Feasible Flexibility Volume

Input: Load forecast $\{l_t\}$, grid limit G, timestep Δt, battery capacity $E_{\max}$, power rating $P_{\max}$
Output: $\{p_t^{\min}, p_t^{\max}, e_t^{\min}, e_t^{\max}\}_{t=0}^{T-1}$
for $t = 0$ **to** $T-1$ **do**
$\quad p_t^{\max} \leftarrow \min\{P_{\max}, G - l_t\};$
$\quad p_t^{\min} \leftarrow \max\{-P_{\max}, -G - l_t\};$
$\quad R^{\mathrm{imp}} \leftarrow 0, \tau \leftarrow t;$
$\quad$**while** $\tau < T$ **and** $l_\tau > G$ **do**
$\quad\quad R^{\mathrm{imp}} \leftarrow R^{\mathrm{imp}} + (l_\tau - G)\Delta t;$
$\quad\quad \tau \leftarrow \tau + 1;$
$\quad e_t^{\min} \leftarrow R^{\mathrm{imp}};$
$\quad R^{\mathrm{exp}} \leftarrow 0, \tau \leftarrow t;$
$\quad$**while** $\tau < T$ **and** $l_\tau < -G$ **do**
$\quad\quad R^{\mathrm{exp}} \leftarrow R^{\mathrm{exp}} + (-G - l_\tau)\Delta t;$
$\quad\quad \tau \leftarrow \tau + 1;$
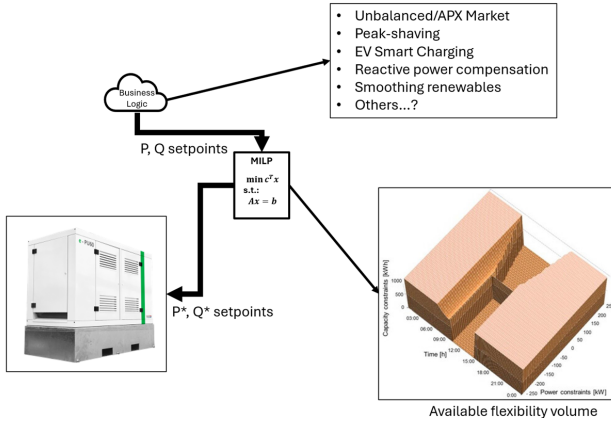$\quad e_t^{\max} \leftarrow E_{\max} - R^{\mathrm{exp}};$

Fig. 1: Overview of the control architecture. High-level business logic generates desired power setpoints, which are adapted by a mixed-integer optimization constrained by the time-varying feasible flexibility volume. The optimized feasible setpoints are then applied to the battery inverter.

B. Setpoint Adaptation via Rolling-Horizon MILP

Once the feasible flexibility volume $\mathcal{V}$ has been constructed, the battery is allowed to follow an external steering signal, denoted p_t^{ref}. This reference signal represents the desired battery power dispatch (e.g., from energy market participation). However, p_t^{ref} may not be feasible with respect to the power and energy constraints defined by $\mathcal{V}$. Therefore, the reference signal is adapted by solving a rolling-horizon mixed-integer linear programming (MILP) problem that determines a feasible power trajectory as close as possible to the desired signal. The MILP ensures that short-term control decisions do not compromise future feasibility, which is not guaranteed if the battery simply clips its power setpoint in real time.

1) Decision Variables: At each time step t within the optimization horizon, the following decision variables are defined:

$$p_t^{\mathrm{in}} \geq 0 \quad \text{(charging)}, \qquad p_t^{\mathrm{out}} \geq 0 \quad \text{(discharging)},$$

$$p_t = p_t^{\mathrm{in}} - p_t^{\mathrm{out}} \quad \text{(net battery power)},$$

$$e_t \quad \text{(battery energy state-of-charge)}.$$

Charging and discharging are modeled separately to allow explicit inclusion of charge and discharge efficiencies.

Objective Function: At each control iteration, an optimization problem is solved over a prediction horizon of length H to ensure that the entire future SoC trajectory remains feasible. The objective, however, penalizes only the deviation between the desired and feasible power at the current time step within the horizon:

$$\min_{\{p_t, e_t\}_{t=0}^{H-1}} (p_0^{\mathrm{ref}} - p_0)^2. \tag{9}$$

This formulation allows the optimizer to consider the full future sequence of constraints (SoC dynamics, power limits, and energy reserves) while focusing the cost function on the immediate control action. The resulting control law is therefore *myopic but constraint-aware*: it guarantees future feasibility without introducing unnecessary optimization bias from future reference values.

Constraints:
a) State-of-Charge Dynamics:

$$e_{t+1} = e_t + \eta\,\Delta t\, p_t^{\mathrm{in}} - \frac{\Delta t}{\eta}\, p_t^{\mathrm{out}}, \tag{10}$$

with the initial SoC e_0 set to the most recent measurement.
b) No simultaneous charge and discharge:

$$p_t^{\mathrm{in}} \cdot p_t^{\mathrm{out}} = 0, \tag{11}$$

implemented in practice using mixed-integer constraints to ensure mutually exclusive charge and discharge operation.
c) Power Limits from Flexibility Volume:

$$p_t^{\min} \leq p_t \leq p_t^{\max}, \tag{12}$$

where $p_t^{\min}$ and $p_t^{\max}$ are derived from the grid headroom constraints (Eq. 2).
d) Energy Limits from Reserve Requirements:

$$e_t^{\min} \leq e_t \leq e_t^{\max}, \tag{13}$$

where $e_t^{\min}$ and $e_t^{\max}$ are computed from the future import and export reserve conditions (Eqs. 4–6).

Rolling-Horizon Implementation: At each real-time control step k:
1) A prediction horizon of length H is established, containing forecasted quantities:

$$\mathcal{H}_k = \{p_{k:k+H-1}^{\mathrm{ref}}, p_{k:k+H-1}^{\min}, p_{k:k+H-1}^{\max}, \\ e_{k:k+H-1}^{\min}, e_{k:k+H-1}^{\max}\}. \tag{14}$$

2) The MILP defined by (9)–(13) is solved over this horizon. The full SoC trajectory ensures future feasibility of the first control action.
3) Only the first control action p_k is applied to the battery (receding-horizon control).
4) The SoC measurement is updated and the horizon is shifted forward for the next iteration.

This approach ensures that at every control step, the battery follows the external reference signal as closely as possible while remaining strictly within the feasible flexibility volume. The forward-looking horizon guarantees that the next control action does not compromise the ability to meet future grid constraints.

C. Forecast-Based and Real-Time Constraint

The constraint management strategy for the battery operation consists of two complementary layers: a *Forecast-Based Constraint (FBC)* layer that defines feasible operation ahead of time using the forecasted grid load, and a *Real-Time Constraint (RTC)* layer that acts directly on the measured grid power flow. Together, these layers ensure that the system remains within the grid capacity limit both in prediction and in reality.

Forecast-Based Constraint (FBC): The FBC layer defines the feasible flexibility volume $\mathcal{V}$ described in Section II-A. It uses forecasts of the building load and grid exchange to determine the expected future power and energy limits. These limits are applied in the mixed-integer optimization problem (Section II-B) to adapt the trading setpoints so that the planned battery operation will not exceed the transformer limit under the forecasted conditions.

Mathematically, this constraint layer enforces:

$$|l_t^{\text{forecast}} + p_t| \leq G, \quad e_t^{\min} \leq e_t \leq e_t^{\max}, \qquad (15)$$

where the bounds are computed from forecast data. The FBC layer thus ensures compliance with expected conditions but cannot prevent violations caused by forecasting errors or unforeseen load fluctuations.

Real-Time Constraint (RTC): The RTC layer complements the forecast-based optimization by continuously monitoring the measured grid power flow l_t^{meas}. If a deviation occurs that would cause $|l_t^{\text{meas}} + p_t| > G$, the RTC immediately overrides the optimized setpoint and adjusts the battery power to maintain the grid connection within its rated limit:

$$p_t^{\text{cmd}} = \begin{cases} G - l_t^{\text{meas}}, & \text{if } l_t^{\text{meas}} + p_t > G, \\ -G - l_t^{\text{meas}}, & \text{if } l_t^{\text{meas}} + p_t < -G, \\ p_t, & \text{otherwise.} \end{cases} \qquad (16)$$

This rule acts as a local safety controller, ensuring that unforeseen short-term deviations or forecast inaccuracies cannot lead to grid overload. In practice, this logic operates at a higher sampling rate than the MILP optimization, directly interfacing with the inverter's power reference.

Hierarchical Control Interaction: The two layers interact hierarchically:

1) The **FBC layer** (forecast-based) generates planned setpoints that satisfy all anticipated constraints.
2) The **RTC layer** (real-time) enforces instantaneous safety by correcting for prediction errors or disturbances.

This layered control ensures that the battery can participate in fast-changing trading signals while protecting the grid interface against constraint violations even under imperfect forecasts. It also enables a clear interpretation of experimental results: the FBC-only case demonstrates the forecast-based flexibility planning, whereas the combined FBC+RTC case illustrates real-time corrective protection.

III. Experimental Setup and Test Scenarios

A. Experimental Setup

The proposed control strategy was validated experimentally using two grid-connected battery systems operated in parallel at laboratory scale. Each battery represented a distinct role within the overall microgrid context:

- **Battery A: Microgrid Battery:** This battery emulated the electrical behavior of an industrial microgrid, including the building load, grid exchange, and grid capacity limit.
- **Battery B: Market Battery:** This battery represented an independently operated system participating in an external energy market. Its reference power signal was a stochastic "trading" steering signal, generated to simulate a time-varying market dispatch request.

Battery B was controlled by the proposed algorithm, while Battery A acted as a controllable background load that influenced the measured grid exchange. The combined operation thus represented an industrial site where market-driven battery control must coexist with physical grid limitations at the point of common coupling.

A building load forecast $\hat{l}_t$ was obtained and used by the Forecast-Based Constraint (FBC) layer to construct the feasible flexibility volume (Section II-A). The FBC then adapted the market steering signal to ensure forecast-based grid compliance. In selected cases, the Real-Time Constraint (RTC) layer was additionally activated to measure and limit the instantaneous grid power in real time.

B. Scenario Definition

To evaluate the algorithm under different operating conditions, three grid-limit configurations were tested:

(i) **Scenario 1: FBC and RTC limits both set to 61 kW.** This scenario establishes a reference case where both predictive and real-time constraints match the true grid limit. This validates that the algorithm does not introduce unnecessary restrictions.
(ii) **Scenario 2: FBC limit set to 20 kW, RTC limit set to 61kW.** This isolates the impact of forecast conservatism: the FBC operates with a tighter virtual limit, while the RTC still monitors the true limit. This case illustrates how the predictive layer can preemptively restrict flexibility to ensure safety under uncertainty.
(iii) **Scenario 3: FBC and RTC limits both set to 20kW.** This scenario combines strict forecast-based and real-time limits, representing the most constrained operation. This case demonstrates the controller's behavior when the available flexibility is significantly reduced.

The nominal grid connection limit of the industrial site is 61 kW, which under normal operating conditions is rarely reached. A lower "virtual" grid limit of 20 kW was introduced to intentionally provoke constraint interactions and to test the system's ability to detect and mitigate potential grid overloads.

Together, these three scenarios allow a systematic assessment of:

- how closely the battery can follow market-driven setpoints under constraint-aware control,
- how effective the FBC is at preventing predicted limit violations, and
- how the RTC responds to unforeseen grid-limit exceedances in real time.

IV. RESULTS

This section presents the experimental results for the three test scenarios described in Section III. For each scenario, we analyze (i) the battery output compared to the external trading setpoint, (ii) the state of charge (SoC) evolution, and (iii) the resulting grid power exchange relative to the applicable grid limits. These visualizations, together with quantitative error and constraint-compliance metrics, illustrate how the layered constraint framework (Forecast-Based Constraint (FBC) + Real-Time Constraint (RTC)) adapts battery behavior in response to forecasted and real-time grid loading conditions.

A. Tracking Performance and Constraint Compliance

Table I summarizes the tracking performance and grid-limit violation reduction across all three scenarios. The tracking Root Mean Square Error (RMSE) is computed relative to the raw market steering signal, not the constraint-adapted setpoint, and therefore quantifies the flexibility sacrifice required to maintain grid safety. Violations refer to any time the grid power would exceed the configured grid limit if the raw market signal were followed directly.

TABLE I: Tracking accuracy and grid-limit violation reduction across scenarios (RMSE computed vs. raw market reference).

Scenario	Samples	RMSE (kW)	Violation Red. (%)
S1 (61/61)	293	6.29	100
S2 (20/61)	9925	13.34	49
S3 (20/20)	463	20.16	100

In Scenario 1, the available grid headroom allowed close tracking of the market-driven setpoint, resulting in low RMSE and complete elimination of grid-limit violations. In Scenario 2, the FBC tightened the feasible flexibility due to anticipated peaks, leading to reduced tracking performance but still a substantial reduction in overload events. In Scenario 3, the grid limit was intentionally restrictive, and the controller appropriately prioritized grid protection, resulting in high RMSE but full violation prevention.

B. Time-Domain Behavior

Figures 2, 3, and 4 show the detailed time-domain behavior for each scenario.

1) Scenario 1: Here, the grid limit was sufficiently high that the external market steering signal was largely compatible with the physical system constraints. As a result, the battery closely followed the requested dispatch signal and maintained a stable SoC trajectory. The grid exchange remained well within limits, demonstrating that in unconstrained conditions the controller introduces no unnecessary restrictions.

2) Scenario 2: In this scenario, the grid-limit constraint in the FBC layer was set more conservatively (20 kW), while the real-time limit remained at 61 kW. This resulted in a more restrictive feasible flexibility volume, especially during periods of high forecasted load. During the second day (May 8, approximately 06:00–16:00), the building load forecast underestimated the actual grid exchange. As a consequence, the controller preserved SoC earlier

(a) Battery output vs. market setpoint

(b) State of Charge (SoC)

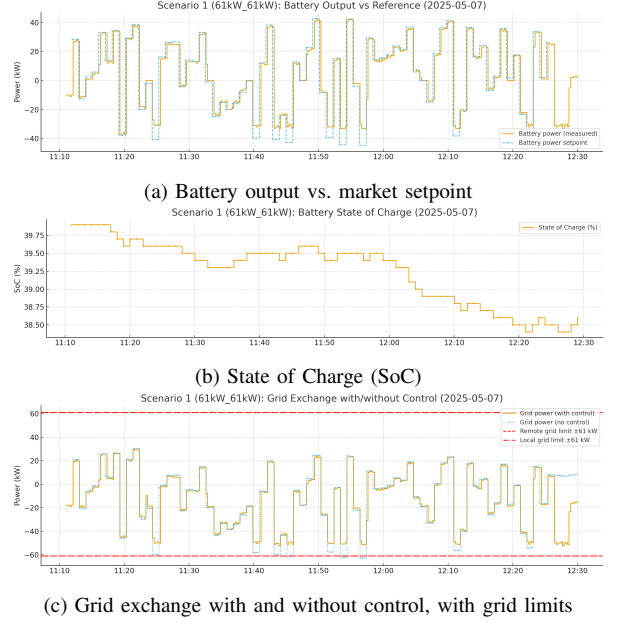(c) Grid exchange with and without control, with grid limits

Fig. 2: Scenario 1 (61 kW / 61 kW): reference tracking under unconstrained transformer headroom.

in anticipation of future peak shaving, but the realized load profile required further discharge than expected. This caused the SoC to drift downward over time, reflecting the controller's attempt to maintain feasibility of future operation despite limited incoming energy opportunities.

Grid-limit violations in Scenario 2 occurred primarily during these periods of forecast inaccuracy. The comparison curve representing the no-control case (market steering signal applied directly) shows significantly larger and more frequent limit breaches. In contrast, the proposed controller successfully mitigated most of these violations by adapting the battery output, reducing violation incidence by approximately 49% (Table I). Thus, the observed behavior aligns with the intended function: the controller follows the external steering signal as closely as possible while respecting the forecasted operational feasibility.

3) Scenario 3: In scenario 3, both the FBC and RTC limits were set to the strict 20 kW threshold. Under such tight grid constraints, even moderate variations in the steering signal would lead to infeasible dispatch if followed directly. The RTC layer therefore intervened frequently to cap the instantaneous grid power flow. This caused the battery to diverge from the market signal and operate in a regime dominated by grid protection, which is reflected in the higher RMSE value in Table I. The restricted operating range also limited the ability of the battery to recharge, leading to a gradual SoC decrease. In this case, the SoC behavior is a direct consequence of the system prioritizing real-time constraint compliance above tracking performance or long-term energy balance.

V. CONCLUSIONS

This paper operationalized the free-flexibility concept introduced by Nykamp et al. within a rolling-horizon MILP and demonstrated its feasibility in real-time operation on physical battery systems using a layered Forecast-Based Constraint (FBC) and Real-Time Constraint (RTC)
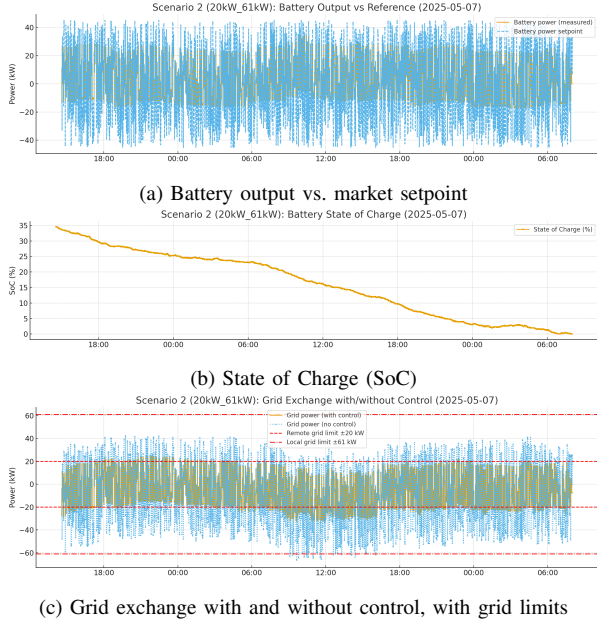
(a) Battery output vs. market setpoint

(b) State of Charge (SoC)

(c) Grid exchange with and without control, with grid limits

Fig. 3: Scenario 2 (20 kW / 61 kW): reduced flexibility due to forecast-based reserve preservation.

(a) Battery output vs. market setpoint

(b) State of Charge (SoC)

(c) Grid exchange with and without control, with grid limits
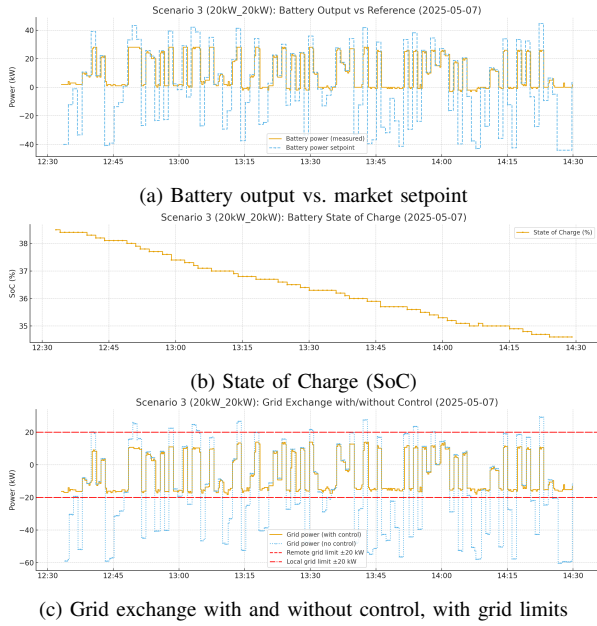
Fig. 4: Scenario 3 (20 kW / 20 kW): strict grid-limit enforcement, fully constrained operation.

structure. The experiments confirm that forecast-based free-flexibility planning can effectively coordinate multi-use battery operation, and that an RTC layer is essential in practice, since forecast uncertainty is unavoidable and can otherwise cause immediate grid-limit violations.

However, the results also show that even with RTC protection, persistent forecast errors and bias lead to gradual state-of-charge drift, eventually reducing tracking capability and forcing frequent corrective actions. In other words, while RTC guarantees instantaneous safety, it does not, on its own, ensure long-term energy balance or stable SoC behavior under realistic uncertainty conditions. This indicates that relying solely on point forecasts in the FBC layer is insufficient for sustained, stable operation.

To address this, the planning layer must be made explicitly uncertainty-aware. Rather than simply improving forecast accuracy, future work will focus on dynamically adjusting reserve margins based on recent forecast error characteristics and incorporating mechanisms that actively recenter the SoC over time. Such adaptations are expected to reduce SoC drift, limit unnecessary RTC interventions, and improve the overall quality of multi-use flexibility provision.

The practical takeaway of this study is that free-flexibility planning is viable and effective when implemented in real-time, but robust operation in the field requires anticipating and managing forecast uncertainty, not just responding to it.

REFERENCES

[1] P. A. N.V., "Financiële impact energietransitie voor netbeheerders ("fien+") — eindrapport," Netbeheer Nederland, Amsterdam, the Netherlands, Tech. Rep., March 2025, in opdracht van Netbeheer Nederland; "Project FIEN+". [Online]. Available: https://bijlagen.nos.nl/artikel-22251257/download.pdf

[2] R. AhmadiAhangar, F. Plaum, T. Haring, I. Drovtar, T. Korotko, and A. Rosin, "Impacts of grid-scale battery systems on power system operation, case of baltic region," *IET Smart Grid*, vol. 7, no. 2, pp. 101–119, 2024. [Online]. Available: https://ietresearch.onlinelibrary.wiley.com/doi/abs/10.1049/stg2.12142

[3] C. Someren, M. Visser, and H. Slootweg, "How battery energy storage impacts grid congestion – an evaluation of the trade-offs between different battery control strategies," *Journal of Energy Storage*, vol. 134, p. 118100, 10 2025.

[4] S. Nykamp, T. Rott, K. Keller, and T. Knop, "Forecast the grid oriented battery operation to enable a multi-use approach and discussion of the regulatory framework," *CIRED - Open Access Proceedings Journal*, vol. 2017, pp. 2760–2763, 10 2017.

[5] J. C. López, J. Reuling, G. Hoogsteen, and J. L. Hurink, "A mathematical framework for digital twins of cyber-physical energy systems." IEEE, 2025, proceedings of an IEEE Conference (exact venue not specified in the PDF).

[6] J. Reuling, J. C. López, G. Hoogsteen, and J. L. Hurink, "Augmented digital twins for microgrid energy management systems: Bridging real-time control and scenario analysis." University of Twente, 2025, conference/venue unspecified.